united nations
educational, scientific
and cultural
organization

international atomic
energy agency

the
abdus salam
international centre for theoretical physics

Winter College on Optics and Photonics
7 - 25 February 2000

1218-12

"Electronic Speckle Pattern Interferometry"

G. SCHIRRIPA-SPAGNOLO
Università Roma Tre
Dipt. Fisica
Italy

ELECTRONIC SPECKLE PATTERN INTERFEROMETRY

GIUSEPPE SCHIRRIPA SPAGNOLO
DIPARTIMENTO DI INGEGNERIA ELETTRONICA
UNIVERSITÀ DI ROMA TRE
ROMA (ITALY)

Contents

Introduction

Electronic Speckle Pattern Interferometry (ESPI) is one of the most common optical methods for deformation testing. This method allows us to measure the full-field surface deformation of a scattering object. It has been used in many fields, among which, the study and characterization of building materials, the assessment of the conservation state of pieces of artwork, and the inspection of civil structures. Besides, an interesting feature of the system is the possibility of grabbing frames continuously from the deforming object and subtracting them in succession from the reference. In this way it is possible to observe the real time evolution of the fringe pattern related to the deformation of the investigated surface.

The surface of an object under test illuminated by a laser appears to have a "speckled" structure of irregular light and dark areas. Waves of laser light scattered by various surface elements are superimposed with a random phase relationship in space. Constructive or destructive interference of the scattered waves leads to this statistical distribution of light and dark areas, known as a speckle pattern.

If the scattered waveform emanating from the diffusing surface of the object is recorded simultaneously with a reference wavefront on the photosensor of a CCD (Charge-Coupled Device) camera, the observed speckle pattern is formed by the interference of two coherent fields and the intensity of resulting field depends on the phase difference between the two fields.

The resulting image of the illuminated object at rest is in fact a speckle pattern very hard to use for subsequent interpretation. If a second speckle pattern of the object at rest is grabbed, it will be exactly identical to the first one. However, when a stress produces a deformation of the order of some micrometer in the surface of the test object, it shifts the phase of the scattered waves. The sensor picks up the resulting change in the speckle brightness. The change in brightness of a particular speckle as the surface is moved from a reference to a deformed state is related to the surface displacement.

In practice, the intensity distribution in the detector plane is stored with the object in its reference state. The object is then deformed and a second frame is stored. The two frames are then subtracted electronically to give a resultant intensity distribution. This looks like an interferogram showing fringes corresponding to the local displacement, but modulated by a superimposed speckle pattern.

The aim of this paper is give the basic notion of the ESPI technique and a brief description of the optical phenomena that are at the base of its operation.

Chapter 1

Principle of superposition and interference of waves

1.1 Intensity

Let $U(x,y,z;t)$ be the analytic signal representation of a single polarization component of the electric field at observation point (x,y,z) and time instant t. For a strictly monochromatic and linearly polarized wave, the analytic signal takes the form[1]

$$U(x,y,z;t) = u(x,y,z)\exp(-2\pi i\nu t), \tag{1.1}$$

where the quantity

$$u(x,y,z) = |u(x,y,z)|\exp[i\phi(x,y,z)], \tag{1.2}$$

is known as the *complex amplitude* of the field.

Since the optical field oscillates at an extremely high rate (ν is of the order of 10^{15} Hz), light detectors (eye- photodiode, CCD, etc.) can measure only the time-averaged value of the optical power per unit area, namely *irradiance* or *intensity*.

Intensity is defined by the energy flux through a unit area per unit time. Therefore, the intensity is proportional to the square of the complex amplitude. Then, neglecting the propor-

tionality factors, we can write

$$I(x,y,z) = \langle U(x,y,z;t)\, U^*(x,y,z;t)\rangle = u(x,y,z)\, u^*(x,y,z) = |u(x,y,z)|^2 , \qquad (1.3)$$

where the asterisk denotes the complex conjugate, and the angular brackets denote a long time average.

1.2 Interference of two waves with equal frequency

The principle of superposition of waves states that if two or more waves of the same nature travel past a given point at the same time, the total amplitude at that point is the sum of the instantaneous amplitudes of the individual waves; a system which obeys this principle is a linear system. We should keep in mind, however, that large-amplitude waves, whether sound waves or high-intensity laser beams, can generate a non-linear response.

In optics, *interference* effects occur if two or more coherent light waves are superposed[2, 3, 4]. We first consider two waves, linearly polarized in the same direction, emitted by the same strictly monochromatic source, with different complex amplitudes. Then the analytic signals associated with the two waves can be written

$$U_1(x,y,z;t) = u_1(x,y,z)\exp(-2\pi i\nu t) = |u_1(x,y,z)|\exp[i\phi_1(x,y,z)]\exp(-2\pi i\nu t) \quad (1.4)$$

$$U_2(x,y,z;t) = u_2(x,y,z)\exp(-2\pi i\nu t) = |u_2(x,y,z)|\exp[i\phi_2(x,y,z)]\exp(-2\pi i\nu t) \quad (1.5)$$

The total complex amplitude is given by

$$U_T(x,y,z;t) = u_1(x,y,z)\exp(-2\pi i\nu t) + u_2(x,y,z)\exp(-2\pi i\nu t) . \qquad (1.6)$$

The intensity is then readily found to be

$$I_T = u_T u_T^* = |u_1|^2 + |u_2|^2 + 2|u_1||u_2|\cos(\phi_1 - \phi_2) . \qquad (1.7)$$

Hence, we can write

$$I_T = I_1 + I_2 + 2\sqrt{I_1 I_2}\cos\left(\phi_1 - \phi_2\right), \tag{1.8}$$

where I_1, I_2 are the intensities of $u_1\left(x,y,z\right)$ and $u_2\left(x,y,z\right)$. For the sake of brevity the dependence of I_1 and I_2 on x,y,z has been dropped.

As can be seen, the resulting intensity is not simply the sum $I_1 + I_2$. One says that the two waves interfere and $2\sqrt{I_1 I_2}\cos\left(\phi_1 - \phi_2\right)$ is called the interference term. The resulting time independent pattern, described by equation (1.8), is called *interference pattern*, the fringes are called *interference fringes.*

Up to now we only have investigated *parallel polarized waves.* The other extreme is the case of *orthogonally polarized waves.* These waves do not interfere, their superposition only leads to the addition of the intensities

$$I_T = I_1 + I_2. \tag{1.9}$$

For other angles between the polarization directions the field vector has to be decomposed into components of parallel and orthogonal polarizations. The result contains interference terms as well as an addition of intensities.

Reasons for the additive intensity term not only may be mutually oblique polarization directions, but also an insufficient coherence of the interfering waves. Because in the superposition of incoherent light we always observe a pure addition of the intensities without interference, the additive term is often called the *incoherent part,* or we speak of *incoherent superposition.*

The visibility of an interference pattern is defined by

$$\text{visibility} = \frac{I_{\max} - I_{\min}}{I_{\max} + I_{\min}} \equiv V, \tag{1.10}$$

where $I_{\max}$ and $I_{\min}$ stand for the maximum and minimum value of the intensity, respectively, when we move across the pattern.

If two parallel polarized waves of the same intensity interfere, we have the maximal visibility of $V = 1$, whereas we have minimal visibility $V = 0$ for incoherent superposition.

1.3 Addition of two Quasimonochromatic Fields

Detection of light (i.e. intensity measurement) is an averaging process in space and time. In developing equation (1.8) we did not average because we tacitly assumed the phase difference $(\phi_1 - \phi_2)$ to be constant in time. This means that we assumed u_1 and u_2 to have the same single frequency. However, sources emitting light of a single frequency do not exist.

Equations (1.4) and (1.5) may be seen as the optical disturbances in the (x, y, z) point due to two different arms of an interferometer (for example a Michelson interferometer) with some path difference, say

$$\ell = c\tau \quad \Longrightarrow \quad \tau = \frac{\ell}{c}, \tag{1.11}$$

where c is the speed of light and τ is the time delay. For a narrow spectral width (i.e. quasi-monocromatic light)[1][5], the complex amplitude varies with time. Therefore, at the observation point we have

$$\begin{aligned} U_1(x,y,z;t) &= u_1(x,y,z;t)\exp([-2\pi i\overline{\nu}t]) \\ &= |u_1(x,y,z;t)|\exp[i\phi_1(x,y,z;t)]\exp(-2\pi i\overline{\nu}t), \qquad (1.12) \\ U_2(x,y,z;t+\tau) &= u_2(x,y,z;t+\tau)\exp[-2\pi i\overline{\nu}(t+\tau)] \\ &= |u_2(x,y,z;t+\tau)|\exp[i\phi_2(x,y,z;t+\tau)]\exp[-2\pi i\overline{\nu}(t+\tau)], \qquad (1.13) \end{aligned}$$

where $\overline{\nu}$ is the average frequency of the light. The overall disturbance at (x, y, z) is

$$U_T(x,y,z;t) = U_1(x,y,z;t) + U_2(x,y,z;t+\tau), \tag{1.14}$$

[1] Quasi-monochromatic light is characterized by the condition that the spectral width of radiation $(\Delta\nu)$ is very small compared to the mean frequency $(\Delta\nu << \overline{\nu})$.

so that the intensity becomes

$$\begin{aligned} I_T(x,y,z) &= \langle U_T(x,y,z;t)\, U_T^*(x,y,z;t)\rangle \\ &= \langle U_1(x,y,z;t)\, U_1^*(x,y,z;t)\rangle + \langle U_2(x,y,z;t+\tau)\, U_2^*(x,y,z;t+\tau)\rangle \\ &\quad + \langle U_1(x,y,z;t)\, U_2^*(x,y,z;t+\tau)\rangle + \langle U_2(x,y,z;t+\tau)\, U_1^*(x,y,z;t)\rangle \\ &= I_1(x,y,z) + I_2(x,y,z) + 2\,\mathrm{Re}\left\{\langle U_1(x,y,z;t)\, U_2^*(x,y,z;t+\tau)\rangle\right\}, \end{aligned} \tag{1.15}$$

where Re denotes the real part.

Since, the complex degree of coherence is defined as

$$\gamma_{12}(\tau) = \frac{\langle U_1(x,y,z;t)\, U_2^*(x,y,z;t+\tau)\rangle}{[I_1(x,y,z)\, I_2(x,y,z)]^{1/2}} = |\gamma_{12}| \exp(i\beta_{12}), \tag{1.16}$$

equation (1.15) can be rewritten as

$$\begin{aligned} I_T(x,y,z) &= I_1(x,y,z) + I_2(x,y,z) \\ &\quad +2\,[I_1(x,y,z)\, I_2(x,y,z)]^{1/2}\, |\gamma_{12}| \cos(\beta_{12}). \end{aligned} \tag{1.17}$$

Equation (1.17) is the generalized interference law for partially coherent quasi-monocromatic light.

Now we can discriminate between perfectly coherent light with $|\gamma_{12}| = 1$ and incoherent light with $|\gamma_{12}| = 0$. For intermediate values of $|\gamma_{12}|$, the radiation is termed partially coherent.

The modulus of the degree of coherence is easily measurable. Indeed if we consider equation (1.17) taking $I_1 = I_2 = I$ we have

$$\begin{aligned} I_{\max} &= 2I\,[1 + |\gamma_{12}|], \\ I_{\min} &= 2I\,[1 - |\gamma_{12}|]. \end{aligned}$$

Therefore the visibility of the fringes, defined by equation (1.10) becomes

$$V = |\gamma_{12}|. \tag{1.18}$$

The visibility is then a measure of the modulus of the complex degree of coherence between the two interfering beams, provided that the intensities of the two beams are identical.

We can introduce the *coherence time* τ_c as the time shift at which the visibility is fallen down to a negligible value[2]. The time shift is realized in interferometers by different optical pathlengths, so one can define the *coherence length*

$$\ell_c = c\tau_c. \tag{1.19}$$

1.4 Coherence length of laser light

Laser light has a rather well-defined wavelength (or frequency). It has nevertheless a certain frequency spread. By spectral analysis of the light, it turns out that it consists of one or more distinct frequencies called resonator *axial modes*, separated by a frequency difference equal to [6]

$$\Delta\nu = \frac{c}{2L} \tag{1.20}$$

where L is the distance between the laser mirrors, i.e. the resonator length. Thus, the spectral distribution of the light from a multimode laser is typically as given in figure 1-1.

For ESPI one often uses He-Ne lasers with internal mirrors. In that case, an important feature of neighboring laser modes, besides their separation, is that their polarization is orthogonal to that of their neighbors (see figure 1-2). Thus, if we examined a three-mode laser (modest power laser produce, usually, only three axial modes) with the appropriate tools, we would find that two of modes have one polarization and the other has a perpendicular polarization. This means that, while axial modes are separated in frequency by $c/(2L)$, modes with the same polarization are separated by c/L.

Now, assume that we use a laser with two axial modes in a interferometerm, for example a Michelson interferometer, whose two arms have a path difference ℓ.

[2]Depending on the spectral properties of the radiation field such value may be zero (see next section) or a suitably small number (e.g., $1/e$).

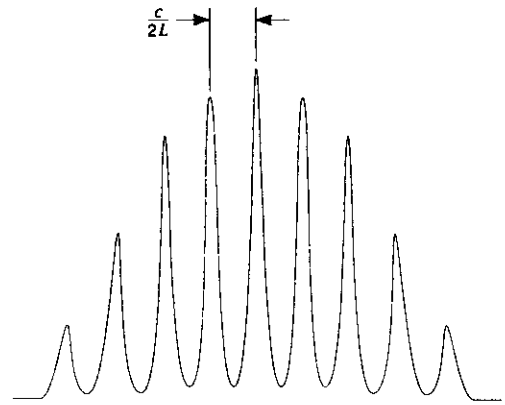

Figure 1-1: Laser mode distribution. Plot of power in laser output as a function of frequency.

We then have two wave fields U_1 and U_2 with frequencies

$$\nu_1 = \frac{c}{\lambda_1} \qquad \text{and} \qquad \nu_2 = \frac{c}{\lambda_2} = \nu_1 + \Delta\nu. \tag{1.21}$$

U_1 will interfere with itself, but not with U_2 and vice versa, and the total intensity thus becomes[3]

$$I_T(\ell) = 2I\left(1 + \cos\frac{2\pi\nu_1\ell}{c}\right) + 2I\left(1 + \cos\frac{2\pi\nu_2\ell}{c}\right), \tag{1.22}$$

where we have assumed U_1 and U_2 to have the same intensity I. Equation (1.22) can be rearranged to give

$$I_T(\ell) = 4I\left[1 + \cos\frac{2\pi(\nu_1 - \nu_2)\ell}{2c}\cos\frac{2\pi(\nu_1 + \nu_2)\ell}{2c}\right]. \tag{1.23}$$

We see that the interference term is the same as that obtained with a light source with

[3] In a Michelson interferometer fed by monochromatic light with wavelength λ we have an intensity distribution given by

$$I_T(\ell) = 2I\left(1 + \cos\frac{2\pi\ell}{\lambda}\right).$$

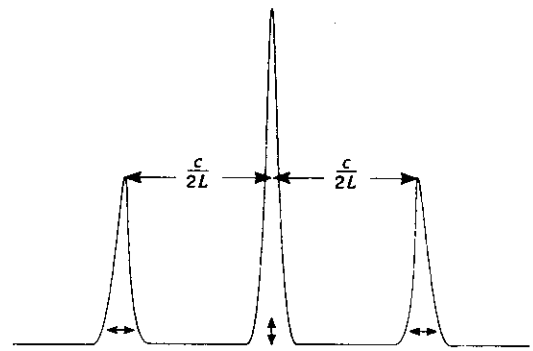

Figure 1-2: Output from a three mode laser. The relative polarization of each mode is indicated at its base.

mean frequency $(\nu_1 + \nu_2)/2$, but multiplied (modulated) by the factor

$$\cos \frac{2\pi (\nu_1 - \nu_2) \ell}{2c}. \tag{1.24}$$

This means that each time

$$\frac{\Delta\nu\ell}{c} = m, \text{ for } m = 0, 1, 2, \ldots \qquad \text{i.e.} \qquad \ell = m\frac{c}{\Delta\nu} = m2L \tag{1.25}$$

the visibility of the interference pattern will have a maximum. The visibility, and therefore the modulus of the complex degree of coherence (see eq. (1.18)), in this case is hence equal to

$$\gamma_{12}(\tau) = \left|\cos \frac{\pi\Delta\nu\ell}{c}\right|. \tag{1.26}$$

The path length difference corresponding to the first minimum of the visibility function (when the argument of the cosine in eq. (1.24) equals $\pi/2$) is

$$\ell_c = \frac{c}{2\Delta\nu} = L, \tag{1.27}$$

which is called the coherence length. This is illustrated in figure 1-3.

When more than two axial modes are oscillating, the result is essentially the same, i.e. the same locations of the minima, but with a more steeply varying visibility function $\gamma_{12}(\tau)$. From

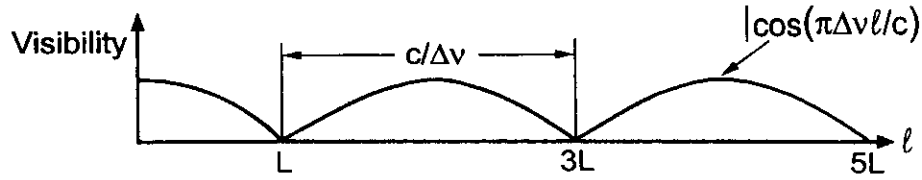

Figure 1-3: Visibility function resulting from two resonator modes of a laser.

this we conclude that when apply a laser in interferometry, the path length difference should be near to zero or to an integer number of twice the resonator length.

Chapter 2

The speckle effect

2.1 Introduction

When a diffusely scattering object is illuminated with coherent light its image has a granular appearance. In Figure 2-1, coherent light is incident on, and scattered from a rough surface with height variations greater than the wavelength λ of the light.

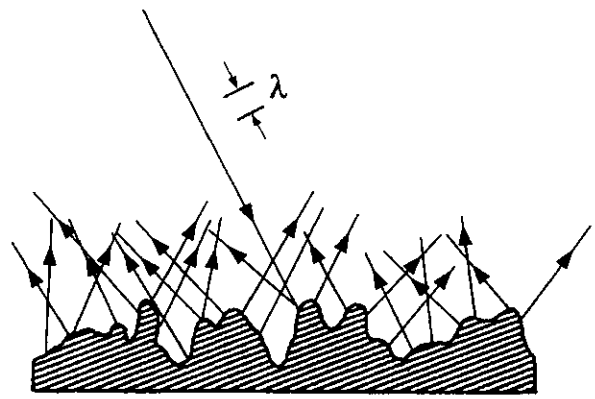

Figure 2-1: Light scattering from a rough surface.

The rough surface can be considered as an ensemble of scattering centers producing scattered wavelets with random phases, which will vary from point to point in proportion to the local surface height. These scattered waves mutually interfere and form an interference pattern consisting of dark and bright spots, called "speckles" [7]. A typical speckle pattern is shown in

Figure 2-2[1].

Figure 2-2: Photograph of a speckle pattern.

There are two types of speckle: Objective and subjective.

An objective speckle pattern is viewed when the light scattered from an object is projected directly onto a screen or the surface of the photodetector without passing through any imaging optics (see Figure 2-3a).

When waves from the scattering medium are imaged by an optical system, the resulting speckle pattern is said to be subjective (see Figure 2-3b). The reason for using this name is that this type of speckle pattern is perceived when a coherently illuminated surface is viewed directly with the eye.

Speckles have known properties which can be advantageous. On the other hand, there are just as many applications where speckles should be eliminated to obtain measurements.

[1] A similar effect occurs in coherent radar and ultrasonic imaging.

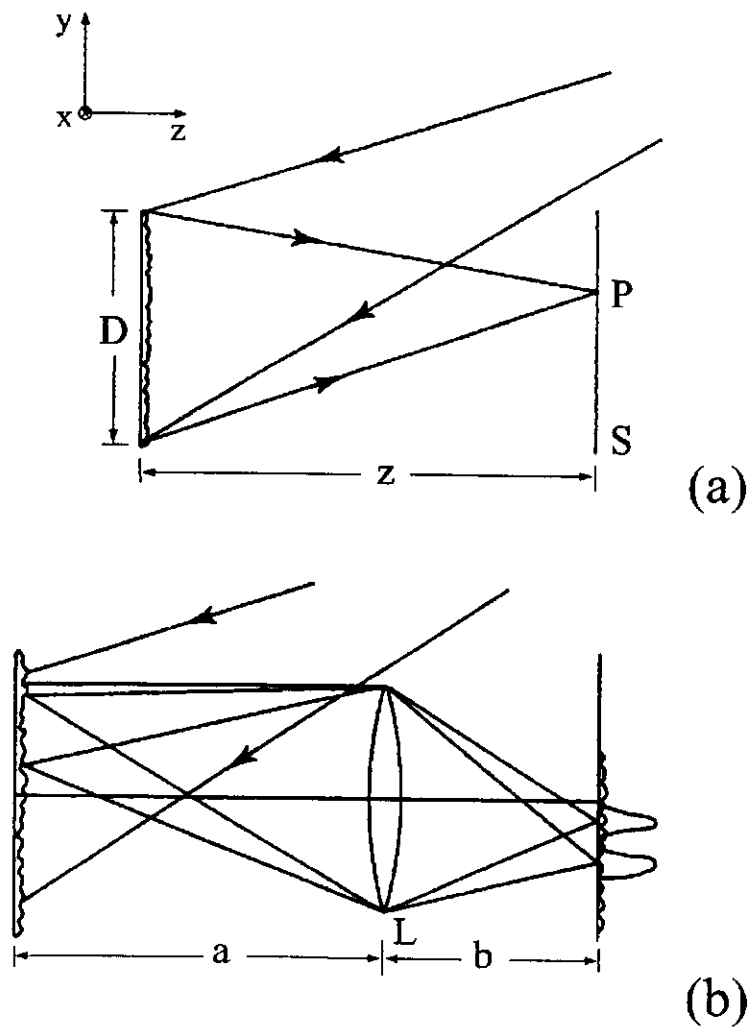

Figure 2-3: Formation of a speckle pattern. (a) Speckle formation in a free-space geometry. (b) Speckle formation in a single-lens imaging system.

2.2 Speckle Properties

The accepted theory of laser speckle makes use of the solution of the well-known statistical problem of the "drunkard's walk". The final position of the random walk is the sum of many independent steps, each of them represented by a displacement vector. For the speckle phenomenon the optical field at an observation point (x, y, z) is made up of a large number, say N, of independent contributions representing the wavelets coming from N elementary areas on the scattering surface. Mathematically, the two cases are identical since the final optical field at (x, y, z) is the vectorial sum of many independent amplitudes associated with the scattered wavelets. The complex amplitude at a typical point in a speckle pattern can therefore be written as

$$u(x,y,z) = \frac{1}{\sqrt{N}} \sum_{k=1}^{N} u_k(x,y,z) = \frac{1}{\sqrt{N}} \sum_{k=1}^{N} U_k(x,y,z) \exp\left[i\phi_k(x,y,z)\right]. \tag{2.1}$$

By assuming that:

1. all components $u_k(x, y, z)$ are mutually coherent and polarized in the same plane;
2. the amplitudes and phases of each component are statistically independent and also independent of the amplitudes and phases of other components;
3. the phases ϕ_k are uniformly distributed between $-\pi$ and $+\pi$;

the complex amplitude of the speckle pattern obeys a circular Gaussian statistics in the complex plane [7]. Essentially, this conclusion can be reached by making use of the central limit theorem. Here, however, we shall simply quote the results of interest.

The probability density function $P_I(I)$ for the intensity in a speckle pattern is given as

$$P_I(I) = \frac{1}{\langle I \rangle} \exp\left(-\frac{I}{\langle I \rangle}\right), \tag{2.2}$$

where $\langle I \rangle$ is the average intensity over many realization of the experiment (the mean intensity). The intensity of the speckle pattern thus obeys negative exponential statistics. Figure 2-4 shows a plot of $P_I(I)$. The most probable irradiance in a speckle pattern is seen to be zero, that is, black. This implies that black speckles are much more likely than bright speckles.

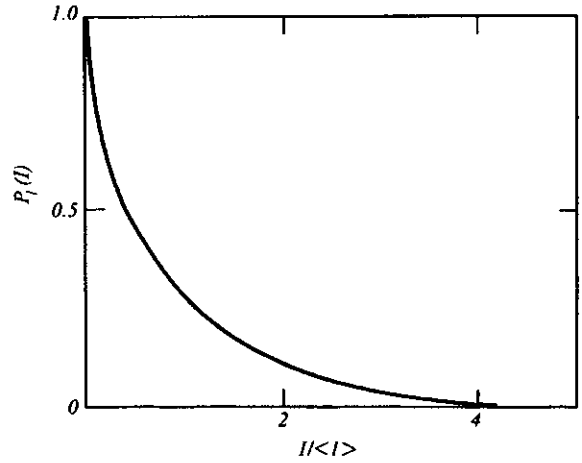

Figure 2-4: Probability density distribution of irradiance in a speckle pattern.

The speckle contrast is defined as the ratio

$$C = \frac{\sigma_I}{\langle I \rangle},$$

where σ_I is the standard deviation of the intensity given by

$$\sigma_I^2 = \left\langle (I - \langle I \rangle)^2 \right\rangle = \left\langle I^2 - 2\langle I \rangle I + \langle I \rangle^2 \right\rangle = \left\langle I^2 \right\rangle - \langle I \rangle^2, \tag{2.3}$$

the brackets denoting again ensemble averages. By using

$$\left\langle I^2 \right\rangle = \int_0^\infty P_I(I)\, I^2 dI = 2\langle I \rangle^2, \tag{2.4}$$

we find the contrast C in a speckle pattern to be unity.

In all the techniques based on a quantitative measurement of the intensity of light scattered by a rough surface, speckle behaves as a noise source. Indeed, its effects are severe, since the signal to noise ratio

$$\frac{S}{N} = \frac{\langle I \rangle}{\sigma_I}, \tag{2.5}$$

equals one whatever the value of $\langle I \rangle$.

2.3 Speckle Size

To find a representative value of the speckle size, consider Figure 2-3a where a rough surface is illuminated by laser light over an area of cross-section D. The resulting objective speckle pattern is observed on a screen S at a distance z from the scattering surface. For simplicity, we consider the intensity variations along the y-direction only. An arbitrary point P on the screen will receive light contributions from all points on the scattering surface. Let us assume that the speckle pattern at P is a superposition of the fringe patterns formed by light scattered from all point pairs on the surface [2]. Any two points separated by a distance ℓ will give rise to fringes of spatial frequency $p = \ell/(\lambda z)$ (see Young's interferometer [1]). The fringes of highest spatial frequency $p_{\max}$ will be formed by the two edge points for which $p_{\max} = D/(\lambda z)$. The period of this patterns is a measure of the smallest objective speckle size σ_o, which therefore equals

$$\sigma_o = \frac{\lambda z}{D}. \tag{2.6}$$

Figure 2-3b shows the same situation as in Figure 2-3a except that the scattering surface is now imaged onto a screen by means of a lens L. The calculation of the size of the resulting subjective speckle is analogous to the calculation of the objective speckle size. Here the linear extent of the illuminated area has to be replaced by the diameter of imaging lens. The subjective speckle size σ_s is therefore given by

$$\sigma_s = \frac{\lambda b}{D}, \tag{2.7}$$

where b is the image distance and D now denotes the lens diameter. By introducing the $f-$number of the optical system $f/\#$

$$f/\# = \frac{f}{D}, \tag{2.8}$$

where f is the focal length, we get

$$\sigma_s = (1 + M)\lambda f/\# \tag{2.9}$$

where $M = (b - f)/f$ is the magnification of the imaging system. From this equation we see that the speckle size increases with decreasing aperture (increasing f-number).

Figure 2-5 shows four different speckle patterns obtained with different $f-$numbers.

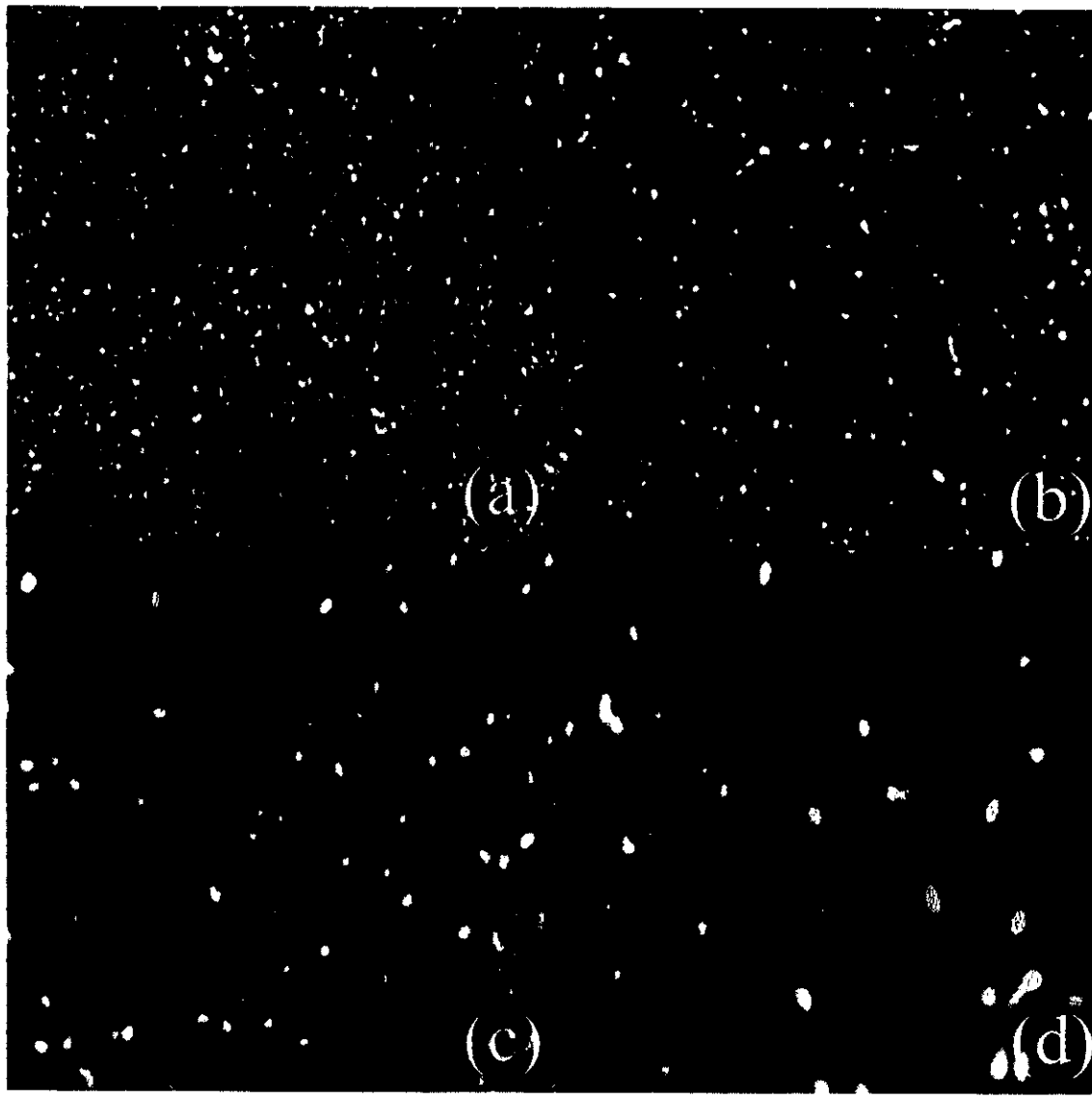

Figure 2-5: Different speckle patterns obtained with different $f-$numbers: (a) $f/8$; (b)$f/16$; (c) $f/32$; (d) $f/64$.

Chapter 3

Electronic Speckle Pattern Interferometry Devices

3.1 Introduction

The electronic speckle pattern interferometry (ESPI; also called TV-holography) was developed in the early 1970's as a method of producing and recording interferometric pattern without using photographic or holographic mediums [8, 9, 10]. It is based on the measurement of changes in a speckle pattern obtained by the coherent superposition of two independent fields, as a function of the phase difference between the two fields.

A speckle pattern, formed by a rough surface illuminated by a laser, is allowed to interfere with a reference wave. This interference pattern is captured by a CCD camera and transferred to a frame grabber on a computer, where it is saved in memory and displayed on a monitor. The resulting image of the illuminated object at rest is a speckle pattern very hard to use for subsequent interpretation. A second speckle pattern of the object at rest will be identical with the first one. However, if the object is slightly deformed, the second speckle pattern is somewhat different.

Comparing both speckle patterns, before and after deformation, information about the surface displacement can be obtained [11].

To sum up, when the object under investigation has been deformed, a second speckle pattern is transferred to the computer and subtracted from the previously stored pattern. The resulting

interferogram is a pattern showing dark and bright fringes, called correlation fringes. An interesting feature of the system is the possibility of grabbing frames continuously while a deformation is occurring and subtracting them in succession from the reference frame. In this way it is possible to observe in real time formation and progressive change of the fringe pattern related to the deformation of the investigated surface.

The whole process: the speckle pattern acquisition, the correlation fringes calculation, and the fringe pattern display is carried out by electronic systems. This was the reason to call it *"Electronic Speckle Pattern Interferometry"*.

Depending on the optical configuration of the ESPI system, it can be made sensitive to out-of-plane displacement, i.e. parallel to the observation direction (see fig. 3-1a), or in-plane displacement, i.e. perpendicular to the line of sight (see fig 3-1b).

3.2 Fundamental concepts

Consider the superposition of two speckle fields in one of the interferometers presented in fig. 3-1. In both setups the coherent light is separated into two components U_1 and U_2.

The complex amplitudes of the wave fronts, at starting steady conditions, in any point (x, y) on the image plane, can be written as

$$U_1(x,y) = |U_1(x,y)| \exp[i\phi_1(x,y)], \tag{3.1}$$

$$U_2(x,y) = |U_2(x,y)| \exp[i\phi_2(x,y)], \tag{3.2}$$

respectively, where $|U_1(x,y)|$ and $|U_2(x,y)|$ are the real amplitudes, $\phi_1(x,y)$ is the phase of the of the arm #1, and $\phi_2(x,y)$ is the phase associated with the arm #2. The speckle pattern, obtained with the test surface in its initial condition (e.g. in the condition that we assume as the reference state), presents an intensity I_{eq}. This intensity distribution, picked up by the

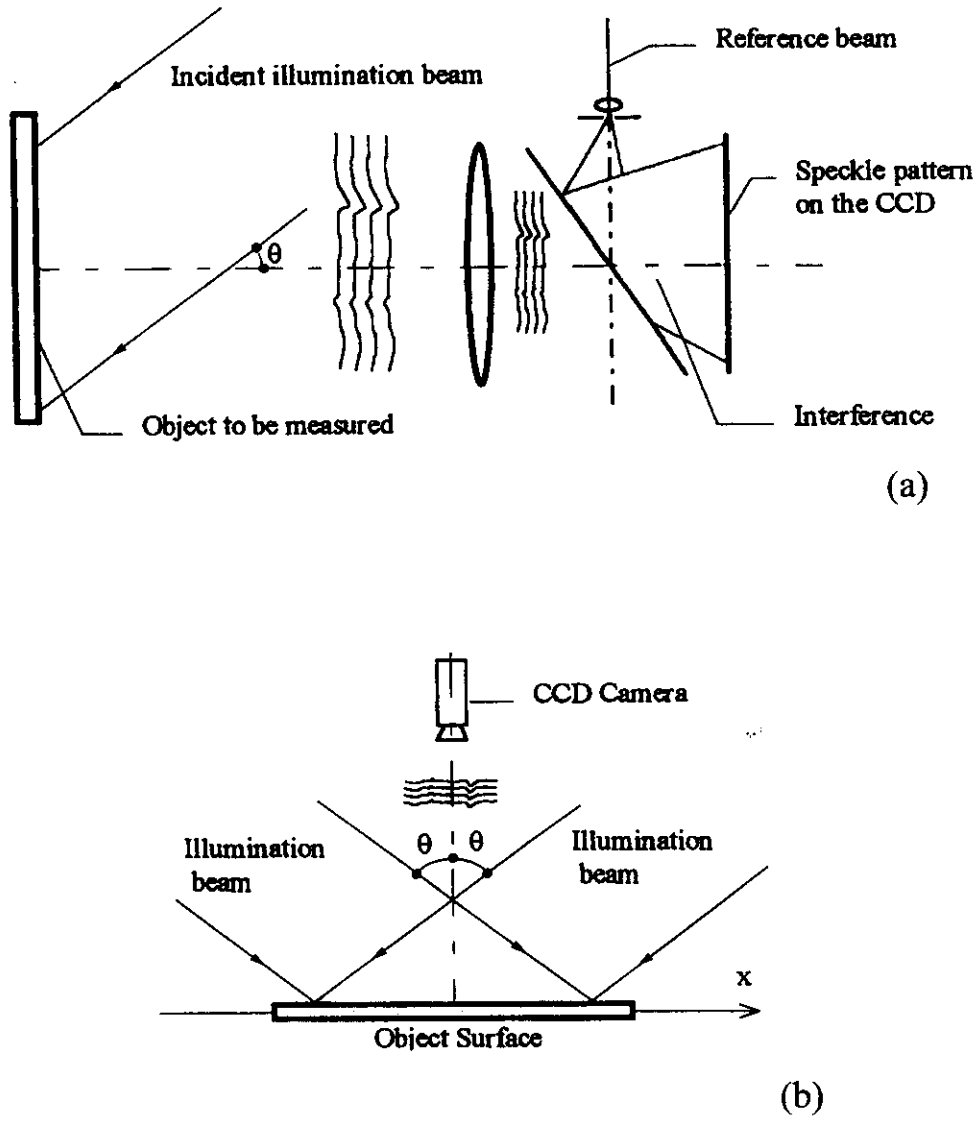

Figure 3-1: (a) typical out-of-plane setup; (b) typical in plane setup.

camera target, is given by the expression

$$\begin{aligned} I_{eq}(x,y) &= |U_1(x,y)|^2 + |U_2(x,y)|^2 \\ &\quad +2\,|U_1(x,y)|\,|U_2(x,y)|\cos\left[\Phi(x,y)\right], \end{aligned} \tag{3.3}$$

where $\Phi(x,y) = \phi_1(x,y) - \phi_2(x,y)$ represents the phase difference between $U_1(x,y)$ and $U_2(x,y)$ due to the two different arms lengths. Because of the surface roughness, $\Phi(x,y)$ varies randomly across the image. It represents the phase of the speckle pattern.

When the object is illuminated, and any displacement occurs, $U_1(x,y)$ phase (out-of-plane) or both $U_1(x,y)$ and $U_2(x,y)$ phases (in-plane) are changed and so $\Phi(x,y)$ turns into $\Phi(x,y) + \varphi(x,y)$.

Consequently, the intensity becomes I_{def} , where

$$\begin{aligned} I_{def}(x,y) &= |U_1(x,y)|^2 + |U_2(x,y)|^2 \\ &\quad +2\,|U_1(x,y)|\,|U_2(x,y)|\cos\left[\Phi(x,y) + \varphi(x,y)\right]. \end{aligned} \tag{3.4}$$

If the phase change $\varphi(x,y)$ is not significantly large, the amplitude of $U_1(x,y)$ and $U_2(x,y)$, and the phase difference $\Phi(x,y)$ are assumed to be the same in eqs. 3.3 and 3.4.

If $\varphi(x,y) = 2n\pi$, then I_{eq} and I_{def} are equal, otherwise the two intensity values are different. Thus, if one image is subtracted from the other, the regions where $\varphi(x,y) = 2n\pi$ will have zero intensity, while other regions will show an intensity randomly varying (i.e. a speckle pattern is obtained) [12].

The interference pattern of eq. 3.4 can be recorded by a CCD camera. In this way, the variations in the texture of the speckles can be converted into a variation of brightness.

If the video signal detected by the CCD is proportional to the light intensities of the speckle image, the output signal from the TV camera, say $B_n(x,y)$, corresponding to the light exposure $I_n(x,y)$ of the nth video frame may be expressed as

$$B_n(x,y) \propto I_n(x,y). \tag{3.5}$$

These image patterns can be digitized and stored in a frame grabber. Then

$$B_{eq}(x,y) \propto I_{eq}(x,y) \quad \text{and} \quad B_{def}(x,y) \propto I_{def}(x,y) \tag{3.6}$$

can be subtracted to obtain speckle fringes [1]. The magnitude of the difference between the two speckle patterns can be displayed on a video monitor. Since the video monitor responds only to positive signals, the subtraction signal is square-law detected before being displayed on the TV monitor. The brightness on the video monitor can be expressed by

$$\begin{aligned} B(x,y) &= [B_{eq}(x,y) - B_{def}(x,y)]^2 \\ &\propto [I_{eq}(x,y) - I_{def}(x,y)]^2 = N(x,y)\, S(x,y)\,, \end{aligned} \tag{3.7}$$

where

$$N(x,y) = 8\,|U_1(x,y)|^2\,|U_2(x,y)|^2\, sin^2\left\{[\Phi(x,y)] + \frac{\varphi(x,y)}{2}\right\}, \tag{3.8}$$

$$S(x,y) = 1 - \cos[\varphi(x,y)]\,. \tag{3.9}$$

Here $N(x,y)$ represents the speckle noise, and $S(x,y)$ describes the fringe pattern [13, 14].

Figure 3-2 shows, schematically, how the fringe pattern of eq. (3.7) is produced by digital subtraction [15].

Equation (3.7) represents a typical ESPI interferogram obtained by subtraction techniques. This interferogram is afflicted with speckle noise that appears as a multiple of tiny spots of varying intensity, superimposed on the true image (the fringe pattern). Figure 3-3 shows a characteristic speckle interferogram of a disbond on an aircraft component.

[1] One tipical limitation in ESPI is that the individual speckles must be resolved by the TV camera. If the separation of the maxima and minima of $\cos[\Phi(x,y)]$ and $\cos[\Phi(x,y) + \varphi(x,y)]$ in eqs. 3.3 and 3.4 is less than the spatial resolution of the TV camera, the last term in these equations will be averaged to zero and no variation will be observed. This requires matching the numerical aperture of the imaging system to a particular sensor. The mean speckle size must be equal to the size of a single pixel of the CCD.

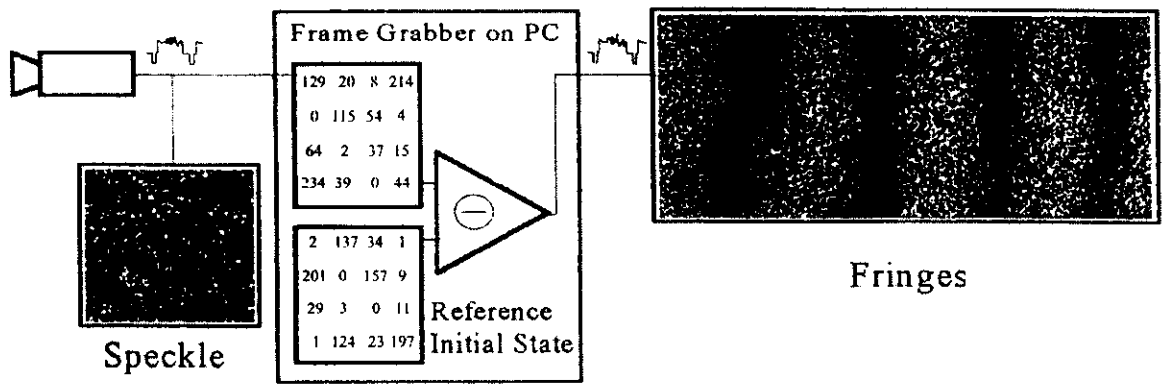

Figure 3-2: Digital subtraction of succesive speckle patterns, and the resulting fringe pattern.

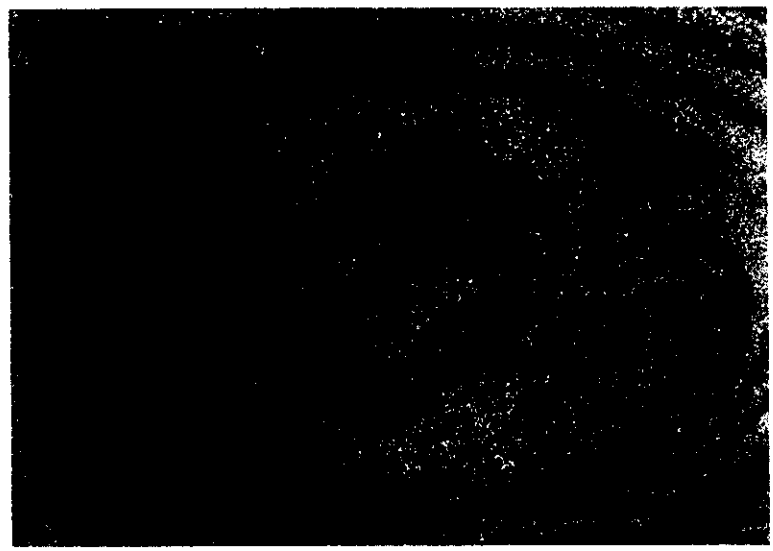

Figure 3-3: A characteristic speckle interferogram.

Assuming that fringe spacing is large enough compared with the mean speckle size, this noise can be considered a high frequency random noise term. Therefore, random speckle noise can be smoothed by using a lowpass filter and a convolution or median window. If we perform an average of the equation (3.7) over all speckle phases (smoothing operation), taking into account the statistical properties of the speckle pattern, we obtain

$$\begin{aligned} \langle B_s(x,y)\rangle &\propto \left\langle [I_{def}(x,y) - I_{eq}(x,y)]^2 \right\rangle = \langle N(x,y)\, S(x,y)\rangle \\ &= \left\langle |U_1(x,y)|^2 \right\rangle \left\langle |U_2(x,y)|^2 \right\rangle \{1 - \cos[\varphi(x,y)]\}. \end{aligned} \tag{3.10}$$

The angular brackets denote ensemble averaging.

Equation (3.10) is equivalent to the classical interferometry equation.

To obtain eq. (3.7) we assumed $|U_1(x,y)|$ and $|U_2(x,y)|$ equal in eqs. (3.3) and (3.4). In practice, the speckles are decorrelated, due to the object deformation as the effective rays collected by the imaging lens are not the same for the first and the second frame [16]. As a consequence, the complex amplitude terms $|U_1(x,y)|$ and $|U_2(x,y)|$ in eqs. (3.3) and (3.4) are not identical and do not cancel out in equation (3.7). Therefore, the fringes visibility is reduced. To take this problem into account, the function $\langle B_s(x,y)\rangle$ can be written as

$$\langle B_s(x,y)\rangle = \left\langle |U_1(x,y)|^2 \right\rangle \left\langle |U_2(x,y)|^2 \right\rangle \{1 - \gamma \cos[\varphi(x,y)]\}, \tag{3.11}$$

where γ is a visibility factor depending on the speckle size and the object deformation.

Equation (3.11) represents the smoothed ESPI interferogram. Since the phase change $\varphi(x,y)$ is a function of the displacement of the surface, information about the relative displacement of different parts of the surface can be obtained.

3.3 Optical geometry in ESPI systems

As we have seen, ESPI systems can be arranged so that the phase change $\varphi(x,y)$ is sensitive to displacement in a particular direction.

The arrangement, shown in fig. 3-4, is commonly used to give fringes which are predominantly related to out-of-plane displacement.

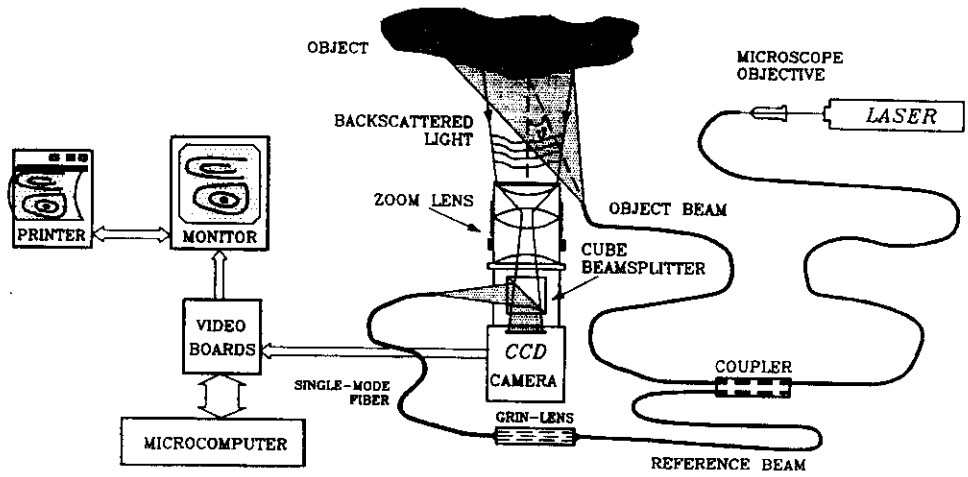

Figure 3-4: An optical ESPI arrangement giving fringes representing out-of-plane displacement.

Coherent light coming from a laser is coupled to a single -mode fiber and a bi-directional coupler splits the incident light into reference and object beams. The object beam diverges from the point S and impinges at a small angle ϑ on the surface. The light scattered from the object is collected by a lens and imaged onto the sensitive area of a TV camera where it mixes coherently by a beam splitter placed located between the imaging lens and the photocathode plane of the TV camera, with the reference beam which diverges from R. The point R would be approximately conjugated with the center C of the viewing lens (e.g., the beam would appear to diverge from C). This is necessary because the interference between the object and the reference beam must not fluctuate at a spatial frequency which is too high to be resolved by the video camera.

In order to satisfy the coherence condition, the optical path difference between the reference and the object beam can be changed by coupling (i.e., through a GRIN lens) a single-mode fiber of appropriate length to the arm of the reference beam (this problem, present with conventional gas laser, is removed utilizing solid state lasers with a long coherence length). Moreover, by controlling the coupling, the intensity ratio of the reference and object wave can be adjusted and adapted to the object reflectivity. Now we consider fig. 3-5, where a point O_N on the object is moved along the displacement vector $\mathbf{d}$ to the point O_D after a deformation of the object. If the displacement $\mathbf{d}$ is considerably smaller than the distance between the object and

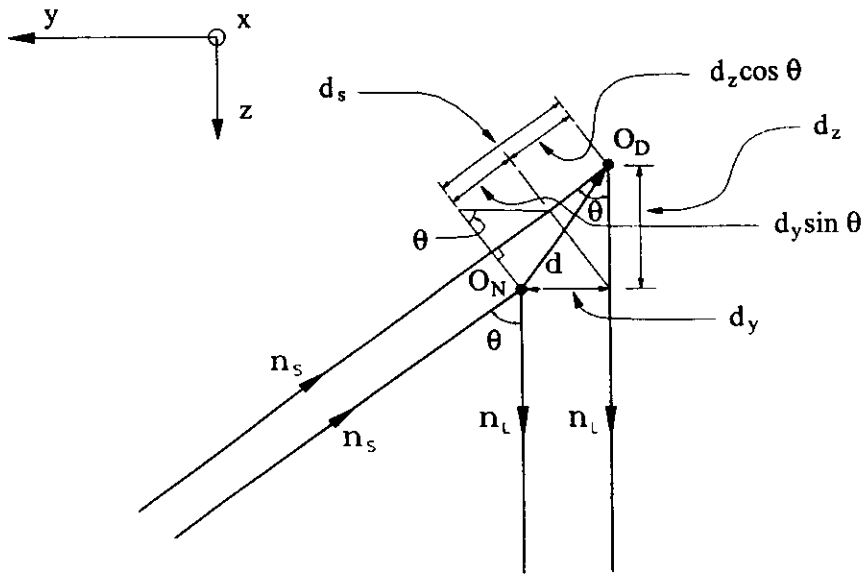

Figure 3-5: The change in optical path associated with a displacement vector **d** (for out-of-plane ESPI interferometer).

the point of divergence S of the illuminating source (or if we use collimated illumination), we can consider the object to be illuminated by a plane wave with the propagation direction $\mathbf{n}_S$. Besides, if **d** is smaller than the distance between the object and the viewing lens, it is possible to assume that the object is looking from infinity along the direction $\mathbf{n}_L$. In this configuration the angle between $\mathbf{n}_S$ and $\mathbf{n}_L$ is ϑ. The geometrical path length from the light source via the object point to the point of observation will be different before and after the deformation has taken place. In our case, this difference is equal to the path length $\Delta l = d_S + d_z$, therefore the phase change is

$$\varphi(x,y) = \frac{2\pi}{\lambda}(d_S + d_z), \tag{3.12}$$

which by simple trigonometric relations becomes

$$\varphi(x,y) = \frac{2\pi}{\lambda}\left[d_z(1+\cos\vartheta) + d_y \sin\vartheta\right], \tag{3.13}$$

where d_z is the out-of-plane displacement and d_y is the in-plane displacement. The possible

displacement in the x direction (with the approximation about the illumination beam and viewing direction mentioned above) does not cause phase change.

If an illumination angle ϑ of at most a few degrees is used, one can put $1 + \cos\vartheta >> \sin\vartheta$ and $\cos\vartheta \approx 1$. Thus we see from eqs. (3.9) and (3.13) that dark fringes are observed in the subtracted speckle pattern when

$$d_z = m\frac{\lambda}{2}\,, \qquad m = 1, 2, 3, 4, \ldots \tag{3.14}$$

Thus, the fringes represent contours of constant out-of-plane displacement.

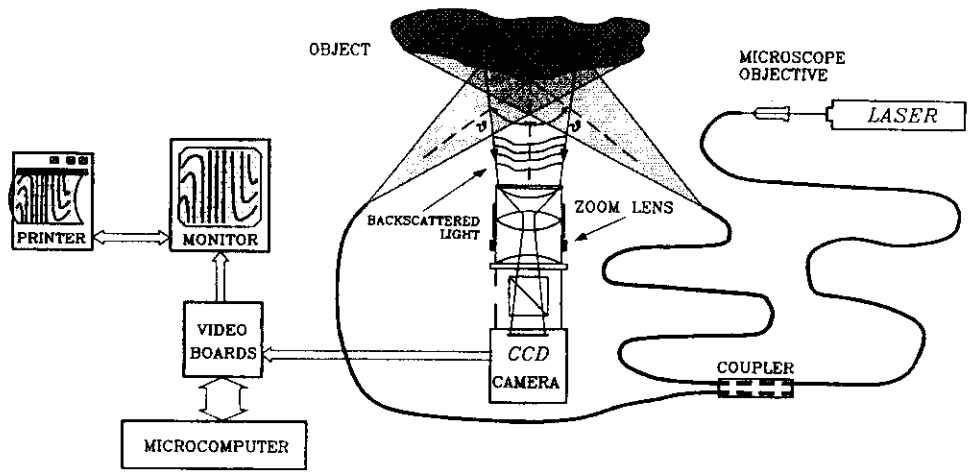

Figure 3-6: An optical ESPI arrangement giving fringes representing in-plane displacements.

An in plane sensitive interferometer can be made by using the apparatus illustrated in fig. 3-6. Here the coherent light coming from a laser is coupled to a single-mode fiber and then amplitude-divided into two beams of equal intensity, which illuminate the object at equal and opposite angle ϑ to the normal surface. The surface is viewed in the normal direction by an imaging lens. The phase change $\Delta\phi_1$ and $\Delta\phi_2$ in the two speckle patterns, due to a general displacement $\mathbf{d}$, are given (with the same approximations about the illumination beam and

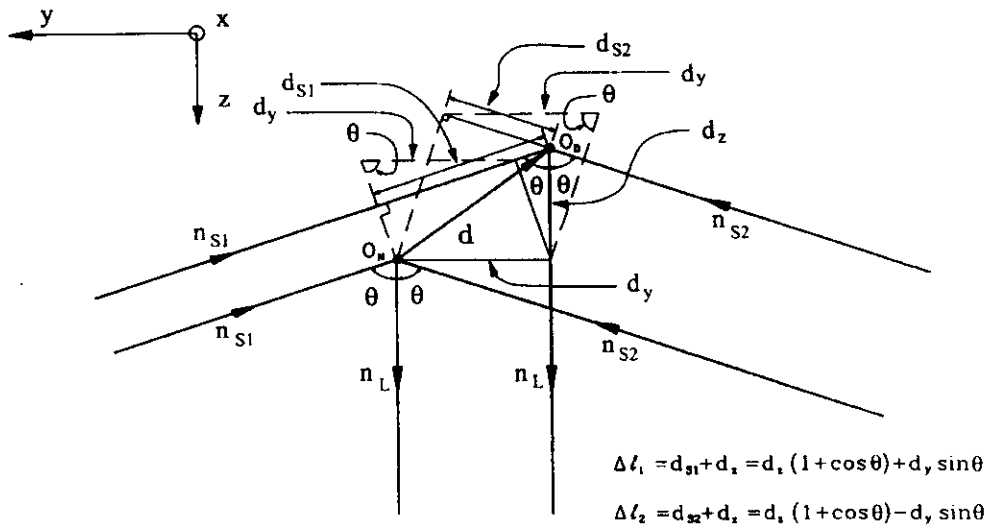

Figure 3-7: Phase change related to a general displacement **d** (for in-plane ESPI interferometer).

viewing direction mentioned above) by (see fig. 3-7)

$$\Delta\phi_1 = \frac{2\pi}{\lambda}\left[d_z\left(1+\cos\vartheta\right) + d_y \sin\vartheta\right], \tag{3.15}$$

$$\Delta\phi_2 = \frac{2\pi}{\lambda}\left[d_z\left(1+\cos\vartheta\right) - d_y \sin\vartheta\right]. \tag{3.16}$$

The possible displacement present in the x direction does not cause change. Hence, the relative phase change between the two back-scattered beams is given by

$$\varphi = \Delta\phi_1 - \Delta\phi_2 = \frac{2\pi}{\lambda}\left(2d_y \sin\vartheta\right), \tag{3.17}$$

and dark fringes are observed in the subtracted patterns when

$$d_y = m\frac{\lambda}{2}\sin\vartheta\ , \qquad m = 1, 2, 3, 4, \ldots\ , \tag{3.18}$$

so that the fringes represent contours of constant in-plane displacement (independent of the presence of out-of-plane displacements).

Chapter 4

Phase Extraction

4.1 Introduction

The fringe patterns represent the displacement of the surface during deformation. Fringes have a sinusoidal intensity profile, it is common to say that a full cycle, a dark and a bright fringe, corresponds to a phase change of 2π. The pixel by pixel analysis of the phase will lead to the determination of the real 3D displacement of the inspected surface.

For quantitative fringe evaluation two methods are commonly used:

- phase shifting;
- Fourier transform method.

4.2 Phase shifting techniques

Phase-shifting is based on the introduction of a known amount of lateral shift, called the phase-step, in the interferometric pattern. The resulting effect is a movement of the intensity values across the pattern. The phase step is introduced as calibrated phase step. The phase change may be implemented in different ways, e.g. a micro-metric movement of a piezoelectric driven mirror, a tilt of a glass plate, an elongation of an optical fibre, a translation of a grating, double refraction in electro-optical modulation, and a refractive index change.

From the computational point of view, a variety of version of the method exist, all of them

sharing the ability to *eliminate* the background and contrast terms by simple arithmetic or trigonometric operations on the acquired images [17].

The phase shifts, however, have to be introduced when the fringes are perfectly still, so the application of phase-shifting techniques is limited only to static or quasi-static deformation measurement.

Phase shifting can be applied to ESPI fringes in a simple and effective manner. The most common phase-shifting technique is one in which the phase change in one arm of the interferometer is divided in N equal and controlled steps so that the total phase shift is 2π.

At each step, a shifted pattern is grabbed. At each shifted speckle pattern corresponds a speckle intensity equation. Using image processing technique and combining the resulting N+1 equations, one eliminates the trivial unknowns in the interference equation to solve for $\varphi(x,y)$.

4.2.1 Phase retrieval

Matematically, one can demonstrate the phase shifting process, starting from eqs. (3.3) and (3.4):

$$\begin{aligned} I_{eq}(x,y) &= |U_1(x,y)|^2 + |U_2(x,y)|^2 \\ &\quad +2\,|U_1(x,y)|\,|U_2(x,y)|\cos\left[\Phi(x,y)\right], \end{aligned} \tag{4.1}$$

with $\Phi(x,y) = \phi_1(x,y) - \phi_2(x,y)$, speckle phase of the reference frame;

$$\begin{aligned} I_{def}(x,y) &= |U_1(x,y)|^2 + |U_2(x,y)|^2 \\ &\quad +2\,|U_1(x,y)|\,|U_2(x,y)|\cos\left[\Phi(x,y) + \varphi(x,y) + \alpha\right], \end{aligned} \tag{4.2}$$

$\Phi(x,y) + \varphi(x,y) + \alpha$ being the sum of the phases relative to the reference frame speckle, the displacement and the phase shift.

The solution may be easily found if we choose for α 3 particular values, $\pi/4$, $3\pi/4$, $5\pi/4$. The selected values produce, after digital subtraction and filtering, three brightnesses that may

be expressed as

$$\begin{aligned}\langle B_s(x,y)\rangle_1 &\propto \left\langle |U_1(x,y)|^2 \right\rangle \left\langle |U_2(x,y)|^2 \right\rangle \{1-\cos[\varphi(x,y)+\pi/4]\} \\ &= \left\langle |U_1(x,y)|^2 \right\rangle \left\langle |U_2(x,y)|^2 \right\rangle \left\{1-\frac{\sqrt{2}}{2}[\cos\varphi(x,y)-\sin\varphi(x,y)]\right\} \quad (4.3)\end{aligned}$$

$$\begin{aligned}\langle B_s(x,y)\rangle_2 &\propto \left\langle |U_1(x,y)|^2 \right\rangle \left\langle |U_2(x,y)|^2 \right\rangle \{1-\cos[\varphi(x,y)+3\pi/4]\} \\ &= \left\langle |U_1(x,y)|^2 \right\rangle \left\langle |U_2(x,y)|^2 \right\rangle \left\{1-\frac{\sqrt{2}}{2}[-\cos\varphi(x,y)-\sin\varphi(x,y)]\right\} \quad (4.4)\end{aligned}$$

$$\begin{aligned}\langle B_s(x,y)\rangle_3 &\propto \left\langle |U_1(x,y)|^2 \right\rangle \left\langle |U_2(x,y)|^2 \right\rangle \{1-\cos[\varphi(x,y)+5\pi/4]\} \\ &= \left\langle |U_1(x,y)|^2 \right\rangle \left\langle |U_2(x,y)|^2 \right\rangle \left\{1-\frac{\sqrt{2}}{2}[-\cos\varphi(x,y)+\sin\varphi(x,y)]\right\} . \quad (4.5)\end{aligned}$$

If the $\left\langle |U_1(x,y)|^2 \right\rangle \left\langle |U_2(x,y)|^2 \right\rangle$ term is even in all the equations, by simple trigonometric operations it is possible to show that the phase can be calculated using

$$\varphi_w(x,y) = \tan^{-1}\frac{\langle B_s(x,y)\rangle_4 - \langle B_s(x,y)\rangle_2}{\langle B_s(x,y)\rangle_1 - \langle B_s(x,y)\rangle_3}. \quad (4.6)$$

4.3 Techniques based on Fourier analysis

The application of Fourier transform techniques to fringe analysis has been the subject of many scientific investigations in the field of interferometric measurements. The interest is justified since the interference phase can be retrieved from one interferogram only. In particular, the Fourier techniques are particularly attractive for a quantitative analysis of the fringes when the measurement is made in difficult environmental conditions (for example in transient phenomena or in presence of external disturbances) [20].

4.3.1 Background concepts

The Fourier transform method [18, 19] is a global operation based on retrieving the phase function in the spatial frequency plane. A phase variation, between complex amplitudes of the current image and of the reference one, is introduced by translation of the object beam. To realize the translation, the fibre, which illuminates the object, is mounted upon a x,z translation stage, adjustable by a piezoelectric device. This shifting causes a carrier spatial frequency modulation to appear, added to the phase difference due to the deformation.

The resulting intensity distribution, say $B_s(x,y)$, of a two-dimensional fringe pattern, can be rewritten as follows

$$\begin{aligned} B_s(x,y) &= N(x,y)E(x,y) = N(x,y)\left\{1-\gamma\cos\left[2\pi\left(f_x x+f_y y\right)+\varphi(x,y)\right]\right\} \\ &= N(x,y)\left\{1-\gamma\frac{1}{2}\exp\left[i\varphi(x,y)\right]\exp\left[i2\pi(f_x x+f_y y\right]\right. \\ &\quad \left.-\gamma\frac{1}{2}\exp\left[-i\varphi(x,y)\right]\exp\left[-i2\pi(f_x x+f_y y\right]\right\}, \end{aligned} \tag{4.7}$$

where f_x and f_y are the linear components of the imposed translation and $\varphi(x,y)$ is the phase change related to the object surface deformation.

The Fourier transform $\mathcal{B}_s(\eta,\xi)$ of the function $B(x,y)$ is the convolution of the signal and noise spectra, i.e.

$$\mathcal{B}_s(\eta,\xi) = \mathcal{N}(\eta,\xi)\otimes\mathcal{E}(\eta,\xi), \tag{4.8}$$

where $\mathcal{N}(\eta,\xi)$ and $\mathcal{E}(\eta,\xi)$ denote the Fourier spectra of $N(x,y)$ and $E(x,y)$, respectively. If $f_0=\sqrt{f_x^2+f_y^2}$ is made larger than twice the largest spatial frequency component of the phase variation, then the Fourier transform of $E(x,y)$ will have three distinct regions of non zero values centred at $\pm f_0$ and at 0 (i.e. DC term)

$$\mathcal{E}(\eta,\xi) = \mathcal{A}_E(\eta,\xi) - \mathcal{C}(\eta-f_x,\xi-f_y) - \mathcal{C}^*(-\eta-f_x,-\xi-f_y), \tag{4.9}$$

with $\mathcal{A}_E(\eta,\xi)$ and $\mathcal{C}(\eta,\xi)$ representing the Fourier transform of 1 and $C(x,y)=\gamma\frac{1}{2}\exp\left[i\varphi(x,y)\right]$, respectively. Roughly speaking, $\mathcal{A}_E(\eta,\xi)$ can be thought of as an impulse. Therefore, it will be

considered a Dirac function $\delta(\eta,\xi)$ in the following.

For a typical speckle pattern, $N(x,y)$ will be a function with rapid local variations but with a slowly varying local mean value. The Fourier spectrum of $N(x,y)$ is

$$\mathcal{N}(\eta,\xi) = \mathcal{A}_N(\eta,\xi) + \mathcal{S}(\eta,\xi). \tag{4.10}$$

In this case too, the sharply peaked function $\mathcal{A}_N(\eta,\xi)$, corresponding to the slowly varying part of $N(x,y)$, can be assimilated to a Dirac function $\delta(\eta,\xi)$. $\mathcal{S}(\eta,\xi)$ denotes the Fourier transform of the fluctuating part of $N(x,y)$.

Hence the spectrum of $B_s(x,y)$ can be written in the form

$$\mathcal{B}_S(\eta,\xi) = \mathcal{A}(\eta,\xi) + \mathcal{C}(\eta - f_x, \xi - f_y) + \mathcal{C}^*(-\eta - f_x, -\xi - f_y) + \mathcal{Q}(\eta,\xi). \tag{4.11}$$

$\mathcal{A}(\eta,\xi)$ is again an impulse-like function arising from the convolution between $\mathcal{A}_E(\eta,\xi)$ and $\mathcal{A}_N(\eta,\xi)$. $\mathcal{Q}(\eta,\xi)$ is the noise floor (the convolution of $\mathcal{S}(\eta,\xi)$ with $\mathcal{C}(\eta,\xi)$ and $\mathcal{C}^*(\eta,\xi)$). If the carrier frequency is small, the speckle noise and the fringe information can be separated in the Fourier plane. In this case, it can be seen that, for values of η and ξ such as either the function $\mathcal{C}(\eta,\xi)$ or the function $\mathcal{C}^*(\eta,\xi)$ is appreciable, the contribution from $\mathcal{A}(\eta,\xi)$ and $\mathcal{Q}(\eta,\xi)$ can be neglected.

The components centred at f_0 can be isolated by a bandpass window. If these components are now shifted by a spatial frequency of $-f_0$, after an inverse Fourier transform, the complex function

$$C(x,y) = \gamma\frac{1}{2}\exp\left[i\varphi\left(x,y\right)\right] \tag{4.12}$$

is obtained. From this equation the phase $\varphi(x,y)$ can be calculated pointwise by the relation

$$\varphi_w(x,y) = \tan^{-1}\frac{\Im\left[C(x,y)\right]}{\Re\left[C(x,y)\right]}, \tag{4.13}$$

where $\Im\left[C(x,y)\right]$ and $\Re\left[C(x,y)\right]$ represent the imaginary and real part of $C(x,y)$.

The phase calculated by eq.(4.13) gives principal values ranging from $-\pi$ to π. The phase distribution is said to be wrapped into this range and 2π jumps occur for variations of more

than 2π.

4.4 Phase unwrapping

Once the phase data have been extracted with phase-shifting or Fourier techniques, final processing is necessary to eliminate the discontinuities which are still present in the wrapped phase map. Phase unwraping consists of preliminary detection of the fringe order, and further reconstruction of the absolute phase jumps between two adjacent fringes. If the difference between two phase of two pixels P_1 and P_2 is greater (or smaller) than a defined threshold (normally taken as π) then it is assumed that the pixels lie in two distinct fringes. The absolute phase value is obtained by adding (or subtracting) 2π to the phase of P_2. Figure 4-1 shows an example of modulo 2π phase calculations and unwrapped phase.

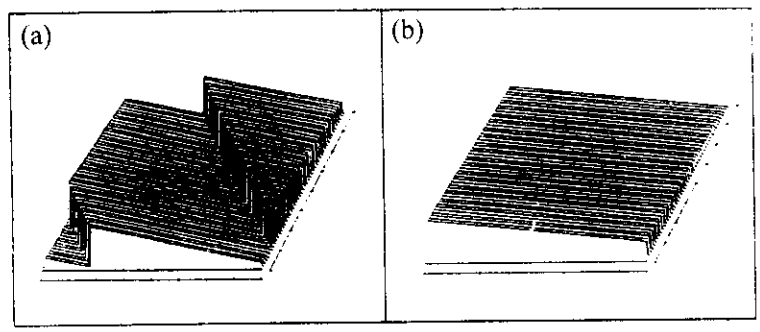

Figure 4-1: (a) modulo 2π phase calculation and (b) unwrapped phase.

The presence of noise or geometrical discontinuities make this process complex and errors are usually difficult to avoid. However, new improved phase unwrapping algorithms are continually being developed to overcome these inefficiencies [21].

Figure 4-2 shows a schematic diagram of the complete procedure of phase extraction by the Fourier method.

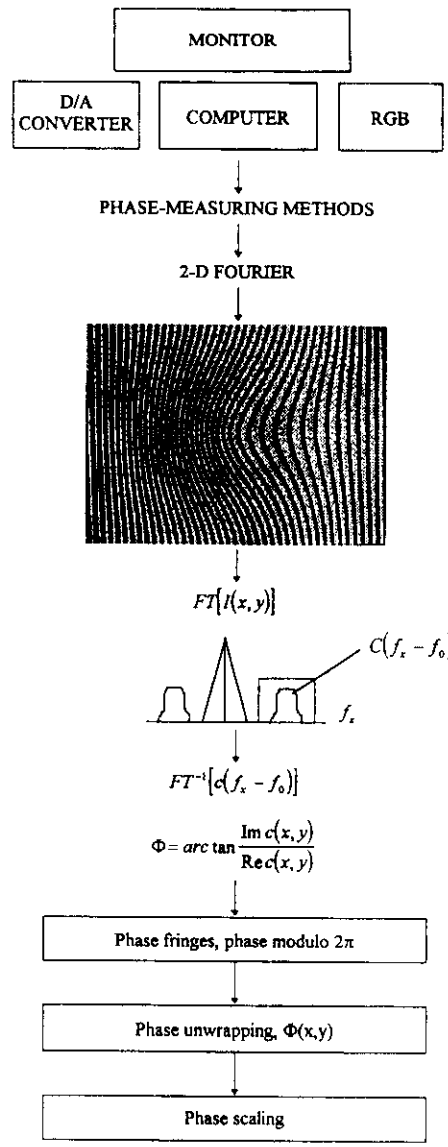

Figure 4-2: Schematic diagram of the complete procedure of phase extraction by the Fourier method.

Bibliography

[1] E. Hecht, *Optics*, Addison-Wesley, Reading-Massachusetts (1987).

[2] K.J. Gåsvik, *Optical Metrology*, John Wiley & Son, Chichester-GB (1987).

[3] M. Born, and E. Wolf E., *Principles of Optics*, Pergamon Press, Oxford (1987).

[4] C.M. Vest, *Holographic Interferometry*, John Wiley & Son, Chichester-GB (1979).

[5] G.O. Reynods, J.B. DeVelis, G.B. Parrent Jr., B.J. Thompson, *Physical Optics Notebook: Tutorial in Fourier Optics*, SPIE, Bellingham (1989).

[6] F.T. Arecchi and Schulz-Dubois, *Laser handbook*, North-Holland, Amsterdam (1972).

[7] J.W. Goodman, "Statistical prôperties of laser speckle patterns", in *Laser Speckle and related phenomena* (ed. J.C. Dainty), pp.9-75, Springer-Verlag, Berlin (1975).

[8] J.N. Butters J.N. and J.A. Leendertz, "Speckle pattern and holographic techniques in engineering metrology", *Opt.Laser Technol.* **3**, 26-30 (1971).

[9] A. Macovski, S.D. Ramsey, and L. F. Schaefer, "Time-lapse interferometry and contouring using television systems", *Appl.Opt.* **10**, 2722-2727 (1971).

[10] O. Schwomma: Austrian Patent 298830 (1972).

[11] R. Jones, and C. Wykes, *Holographic and Speckle Interferometry*, 2nd ed., Cambridge University Press, Cambridge (1989).

[12] P. Zanetta, Ph.D. Thesis Loughborough University of Technology (UK) Technical Note ISEI/IE/2777/94, Commission of the European Communities, Joint Research Centre, Ispra Site (1994).

[13] D. Paoletti, G. Schirripa Spagnolo, M. Facchini, and P. Zanetta ,"Artwork Diagnostics with Fiber Optics DSPI", *Appl. Opt.* **32**, 6236-6241 (1993).

[14] D. Paoletti, and G. Schirripa Spagnolo, "Interferometric methods for artwork diagnostics", *Progress in Optics* **XXXV**, 197-255 (1996).

[15] D. Albrecht, Ph.D. Thesis Loughborough University of Technology (UK) Special Publication No. I.99.40, Commission of the European Communities, Joint Research Centre, Ispra Site (1999).

[16] M. Owner-Petersen, "Decorrelation and fringe visibility: on the limiting behavior of various electronic speckle-pattern correlation interferometers", *J. Opt. Soc. Am. A* **8**, 1082-1089 (1991).

[17] C. Creath, "Phase-measurement interferometry techniques", *Progress in Optics* **XXVI**. 349-393 (1988).

[18] M. Takeda, H. Ina, and S. Kobayashi, "Fourier transform method of fringe pattern analysis for computer based topography and interferometry", *J. Opt. Soc. Am.* **72**, 156-160 (1982).

[19] R.N. Bracewell, *The Fourier Transform and Its Applications*, McGraw-Hill, New York (1986).

[20] T. Kreis, *Holographic Interferometry*, Akademie Verlag, Berlin (1996).

[21] D.W.Robinson, "Phase Unwrapping Methods", in *Interferogram Analysis: digital fringe pattern measurement techniques*,(eds D.W. Robinson and G.T. Reid), IOP Publishing, Bristol (1993).